Crucial role of doping dynamics on transport properties of Sb-doped SnO_2 nanowires

Annop Klamchuen,[1,2] Takeshi Yanagida,[1,3,a)] Kazuki Nagashima,[1] Shu Seki,[3,4] Keisuke Oka,[1] Masateru Taniguchi,[1,3] and Tomoji Kawai[1,a)]
[1]Institute of Scientific and Industrial Research, Osaka University, 8–1 Mihogaoka, Ibaraki, Osaka 567-0047, Japan
[2]NANOTEC, NSTDA, 111 Thailand Science Park, Paholyothin Rd. Klong 1, Klong Luang, Pathumthani 12120, Thailand
[3]PRESTO, Japan Science and Technology Agency, 4-1-8 Honcho, Kawaguchi, Saitama 332-0012, Japan
[4]Division of Applied Chemistry, Graduate School of Engineering, Osaka University, 2-1 Yamadaoka, Suita, Osaka 565-0871, Japan

(Received 10 June 2009; accepted 2 July 2009; published online 4 August 2009)

Impurity doping on semiconductor nanowires grown by vapor-liquid-solid (VLS) mechanism remains an important challenge. Here we demonstrate the importance of doping dynamics to control the transport properties of Sb-doped SnO_2 nanowires. Sb doping decreased the resistivity of SnO_2 nanowires down to 10^{-3} Ω cm range, while there was the lower bound of resistivity even increasing further the dopant concentration from supplied source. We found that the doping limitation is related to the re-evaporation events of dopant through vapor-solid growth process rather than VLS process. Thus understanding the dopant incorporation dynamics is essential to control the transport properties of SnO_2 nanowires by impurity doping. © *2009 American Institute of Physics*.
[DOI: 10.1063/1.3186080]

Semiconductor nanowires grown via the vapor-liquid-solid (VLS) mechanism are attracting much attention due to not only the nanoscale scientific interests but also the potential device applications.[1] Impurity doping is an important process to control the transport properties of semiconductors. Feasibility of the impurity doping for VLS grown nanowires has been intensively investigated due to the complex nature of dopant incorporation dynamics.[2] The essential difference between VLS grown nanowires and thin films on the impurity doping is the presence of a metal catalyst, which is a liquid state during VLS, and the mass transport events through liquid-solid, vapor-liquid, and vapor-solid (VS) interfaces. Thus the complex dynamics of the impurity doping on VLS growth has held back the arbitral controllability of the electric properties. Although the dopant incorporation processes on growths of nanowires comprised of single element including Si and Ge are complex enough,[2–4] the doping process for nanowires comprised of multielements would be more complex. Although metal oxides exhibit many interesting physical properties,[5] current knowledge as to the impurity doping on VLS grown oxide nanowires is still scarce and far from the comprehensive understanding. For example, impurity-doped SnO_2 nanowires by VLS have been investigated due to the transparent conductivity of $SnO_{2-\delta}$.[6] The wide variation of the measured conductivity was found;[6] however, the mechanism of such wide variation has not been identified due to the lack of understanding of the dopant incorporation process. In addition, the uniform dopant distribution within nanowires has been assumed in previous investigations.[6] The lack of understanding and the variation of transport properties would be detrimental for the reliable device applications. These backgrounds motivated us to investigate the transport properties of Sb-doped SnO_2 nanowires grown by VLS and the dopant incorporation mechanisms. Our results highlight the crucial role of dopant incorporation dynamics on the transport properties of Sb-doped SnO_2 nanowires.

SnO_2 nanowires were grown on Al_2O_3 (110) single crystal substrate by Au catalyst-assisted pulsed laser deposition technique (ArF excimer laser, $\lambda = 193$ nm).[7] The background pressure of the chamber was 10^{-5} Pa. Sn and Sb_2O_3 mixed powders (Koujundo Chemical) were used as the target with varying the Sb dopant concentration. The Sb dopant concentration (at. %) is hereafter defined as the atomic ratio of Sb to Sn. Oxygen and argon mixed gas was introduced into the chamber with controlling the ambient total pressure 10 Pa with the flux ratio of oxygen and argon (1:1000). Prior to the laser ablation, the Au-coated Al_2O_3 substrate was preheated at 750 °C for 20 min. The typical growth temperature was

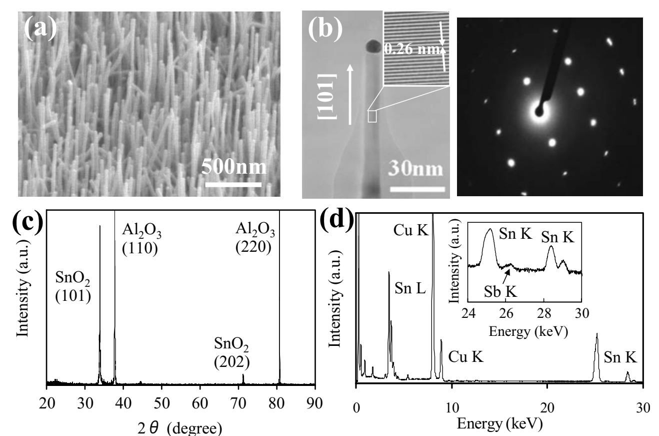

FIG. 1. (a) FESEM image of Sb (5 at. %)-doped SnO_2 nanowires. (b) HRTEM image and SAED pattern. (c) X-ray diffraction (XRD) data. (d) EDS data. The inset shows the data around Sn *K* and Sb *K* shell peaks.

a)Authors to whom correspondence should be addressed. Electronic addresses: yanagi32@sanken.osaka-u.ac.jp and kawai@sanken.osaka-u.ac.jp.

 © 2009 American Institute of Physics

Downloaded 07 Aug 2009 to 133.1.58.105. Redistribution subject to AIP license or copyright; see http://apl.aip.org/apl/copyright.jsp

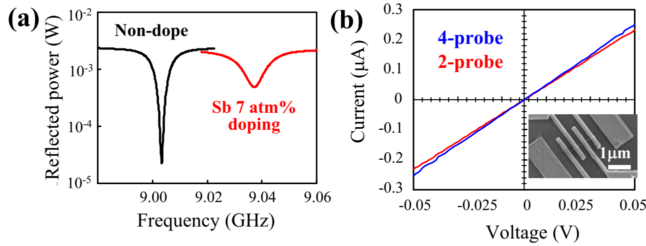

FIG. 2. (Color online) (a) Resonance curves of MCM. Data of nondoped system and Sb (7 at. %)-doped SnO_2 nanowires were shown. (b) *I-V* curves measured by FPCM for Sb (7 at. %)-doped SnO_2 nanowires. Two-probe and four-probe data were shown. The inset shows FESEM image of FPCM device structure.

750 °C. The nanowire morphology was characterized by field emission scanning electron microscopy (FESEM) (S-4300) at an accelerating voltage of 30 kV. High-resolution transmission electron microscopy (HRTEM) (JEM-3000F) coupled with energy dispersive spectroscopy (EDS) at an accelerating voltage of 300 kV was used to evaluate the diameter, the crystallinity, and the composition of the fabricated nanowires. We employed two different methods to measure the transport properties of nanowires, including a microwave conductivity measurement (MCM) and a four-probe conductivity measurement (FPCM). Detail apparatus of MCM can be seen elsewhere.[7,8] All the above experiments were carried out at room temperature in Ar or SF_6 atmosphere. For FPCM, we utilized devices composed of individual nanowires, which were fabricated by combining photolithography and electron-beam (e-beam) lithography processes. Then the metal deposition of Pt/Au 20/100 nm were carried out. The transport properties were measured by using semiconductor analyzer (Keithley 4200).

Figure 1(a) shows the typical FESEM image of Sb-doped SnO_2 nanowires grown on Al_2O_3 (110) substrate. The Sb composition in the target was 5 at. %. It can be seen that the fabricated SnO_2 nanowires grow almost perpendicular to the substrate. The presence of nanowire growth was consistently confirmed for the range of Sb-concentration (1–7 at. %) in the target. Figure 1(b) shows the HRTEM image of fabricated SnO_2 nanowire and the selected area electron diffraction (SAED) pattern. The single crystalline nature and (101) oriented growth of fabricated SnO_2 nanowires can be seen. X-ray diffraction (XRD) data also supports the (101) oriented growth, as shown in Fig. 1(c). Figure 1(d) shows the EDS data in HRTEM, which indicates the presence of Sb dopant within nanowires. Note that it is crucial to identify the presence and the concentration of Sb dopant within nanowires via Sb *K* shell peaks rather than Sb *L* shell peaks due to the significant overlapping of Sn and Sb peaks. The estimated Sb concentration was almost 2 at. %, which is smaller than the nominal value 5 at. %. Figure 2(a) shows the absorption curves of MCM for nondope SnO_2 nanowires and Sb (7 at. %)-doped SnO_2 nanowires. The attenuation factor Q around the resonance for Sb-doped nanowires was found to be much larger than that of nondope nanowires, indicating that the conductivity of Sb-doped nanowires is higher. Figure 2(b) shows the typical data of current (I) versus voltage (V) of FPCM for Sb (7 at. %)-doped SnO_2 nanowire. The inset of Fig. 2(b) shows the FESEM image of fabricated device structure. The linear relationship of *I-V* data was seen in both two-probe and four-probe configurations, indicating the Ohmic contact. In addition, the *I-V* data obtained from the two-probe method is almost identical to that obtained from the four-probe method. Table I shows the comparison between MCM and FPCM in the resistivity data for both nondope and Sb (7 at. %)-doped SnO_2 nanowires. The reasonable agreement between MCM and FPCM data can be seen. The agreement between ac and dc measurements is theoretically understandable[8] when considering the mobility range of impurity-doped SnO_2, which is typically ranged from 20–50 $cm^2\ V^{-1}\ s^{-1}$.[9] Note that the MCM data is an averaged value of 10^{11} nanowires. Thus the reliable transport data of MCM affords us to focus our studies on the MCM data in the following discussions.

TABLE I. Comparison between MCM and FPCM on the resistivity data of nondope SnO_2 nanowires and Sb (7 at. %)-doped SnO_2 nanowires.

	Resistivity at RT (Ω cm)	
	MCM	FPCM
Nondope	6.67×10^{-1}	3.86×10^{-1}
Sb: 7 at % in target	4.35×10^{-3}	7.12×10^{-3}

Figure 3 shows the dependence of supplied dopant concentration on the resistivity. Interestingly there was the lower bound of resistivity even increasing further the dopant concentration from supplied source above 3 at. %. The inset shows the Sb concentration data within nanowires, demonstrating that the incorporated dopant concentration approached the limited value around 2 at. % above 3 at. % of supplied dopant concentration. Clearly there is a reasonable correspondence between the resistivity and the incorporated dopant concentration. As such the lower bound of resistivity is closely related to the dopant incorporation dynamics. The dopant incorporation dynamics is related to three major processes, including (1) the supplied process of dopant from the source, (2) the re-evaporation process of supplied dopant from the surface, and (3) the dopant incorporation process into nanowires. We examined the effects of each process in the following discussions. First in (1), the supplied process, the dopant concentration supplied onto the surface was investigated by measuring the dopant concentration of thin films formed under RT, where the re-evaporation process is negligible. The electron probe microanalysis on the Sb (20 at. %)-doped SnO_2 films demonstrated that the dopant concentration within the film was 20.07 at. %, which is almost identical to the nominal value. Thus there is no significant difference between the dopant concentration supplied onto the surface and the nominal dopant concentration in the present experiments. Second, the re-evaporation process of dopant on the surface was studied by measuring the dopant

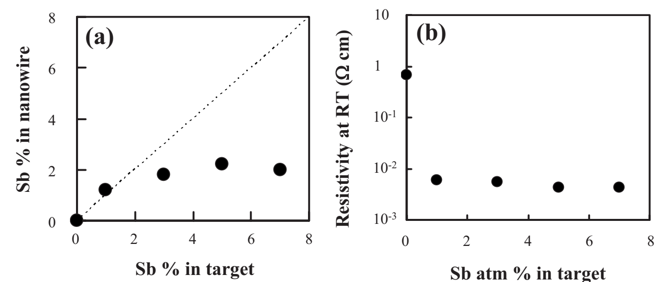

FIG. 3. (a) The Sb concentration data within nanowires by EDS when varying the supplied dopant concentration. (b) Dependence of supplied dopant concentration on the resistivity measured by MCM.

Downloaded 07 Aug 2009 to 133.1.58.105. Redistribution subject to AIP license or copyright; see http://apl.aip.org/apl/copyright.jsp

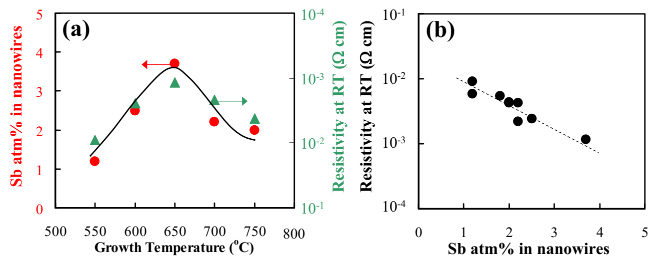

FIG. 4. (Color online) (a) Dopant concentration data within nanowires and resistivity data when varying the growth temperature from 550 to 750 °C. (b) Relationship between the incorporated dopant concentration and the resistivity of nanowires for various conditions.

concentration of thin films grown at 400 °C. The remaining dopant concentration within the film was 1.73 at. %, which is much lower than the nominal value 20 at. %. Although above experiments were performed in the absence of Au catalysts, the re-evaporation process must be substantial when performing a nanowire growth above 400 °C. Based on above experimental implications, an enhancement of the dopant incorporation might be achieved by decreasing the growth temperature, i.e., the reduction of re-evaporation events. Figure 4(a) shows the dopant concentration data within nanowires when varying the growth temperature from 550 to 750 °C. Note that there was no SnO_2 nanowire growth below 550 °C. The nominal dopant concentration in supplied source was 5 at. %. The significant enhancement of dopant incorporation was observed when reducing the growth temperature from 750 to 650 °C. The dopant concentration within nanowires grown under 650 °C was nearly 4%, which is in fact twice when compared with the value for 750 °C. As such the reduction of re-evaporation process can be achieved by controlling the nanowire growth temperature. Further decreasing the growth temperature from 650 to 550 °C resulted in the decrease of the dopant concentration within nanowires. This is presumably due to (i) the suppression of diffusion length of dopant adatoms on the surface and (ii) the presence of an activation energy barrier for incorporating dopant adatoms into nanowires. Although Sb re-evaporation from the SnO_2 nanowire surface must occur, our results indicate the dominance of Sb re-evaporation events before the dopant incorporation process rather than the re-evaporation from the solid surface. Figure 4(a) also shows the resistivity data of nanowires when varying the growth temperature. Clearly there is a remarkable correspondence between the incorporated dopant concentration and the conductivity of nanowires when varying the growth temperature. Figure 4(b) summarizes the relationship between the incorporated dopant concentration and the resistivity of nanowires for various conditions. The reasonable correspondence can be seen. Thus it is very important to control the dopant incorporation process rather than varying the supplied dopant concentration. Further remained issue is the dopant incorporation pathway. There are two distinct incorporation pathways of dopant adatoms, including a VLS process via metal catalysts and a VS process through the nanowire surface. The VS mechanism assumes the inhomogeneous dopant distribution within nanowires,[4] whereas the VLS mechanism assumes the homogeneous dopant distribution. Assuming the homogeneous dopant distribution within nanowires, the experimental data of resistivity should agree with theoretical value estimated by the following formula: $\rho=1/e\mu n$, where e is an elementary electric charge, μ is a mobility, and n is a carrier density. Adapting the data of the μ (40–50 $cm^2\ V^{-1}\ s^{-1}$) and n $[(3.0–8.0)\times 10^{20}\ cm^{-3}]$ for our experimental configurations,[6,9] the theoretical value is ρ_{theory}:$(1.7–5.2)\times 10^{-4}$ Ω cm, which is an order of magnitude lower than our experimental value ρ_{exp}:4.3×10^{-3} Ω cm. The discrepancy cannot be solely explained in terms of the variation of μ and n data for the estimation. Thus this indicates the inhomogeneous dopant distribution within nanowires, in other words, the dominance of VS incorporation mechanism rather than the VLS. Recently Lauhon and co-workers[4] reported such inhomogeneous dopant distribution of P-doped Ge nanowires with the relation to the differences in precursor decomposition rates, and the similar mechanisms might govern our experimental system. These results highlight that understanding the dopant incorporation dynamics is rather essential to control appropriately the transport properties of SnO_2 nanowires by impurity doping.

This work is partially funded by SCOPE.

[1]C. M. Lieber and Z. L. Wang, MRS Bull. **32**, 99 (2007).
[2]E. C. Garnett, Y. C. Tseng, D. R. Khanal, J. Wu, J. Bokor, and P. D. Yang, Nat. Nanotechnol. **4**, 311 (2009).
[3]M. Law, J. Goldberger, and P. D. Yang, Annu. Rev. Mater. Res. **34**, 83 (2004).
[4]D. E. Perea, E. R. Hemesath, E. J. Schwalbach, J. L. Lensch-Falk, P. W. Voorhees, and L. J. Lauhon, Nat. Nanotechnol. **4**, 315 (2009); J. E. Allen, D. E. Perea, E. R. Hemesath, and L. J. Lauhon, Adv. Mater. **21**, 2098 (2009); D. E. Perea, E. Wijaya, J. L. Lensch-Falk, E. R. Hemesath, and L. J. Lauhon, J. Solid State Chem. **181**, 1642 (2008).
[5]T. Yanagida, T. Kanki, B. Vilquin, H. Tanaka, and T. Kawai, Phys. Rev. B **70**, 184437 (2004); T. Yanagida, H. Tanaka, T. Kawai, E. Ikenaga, M. Kobata, J. Kim, and K. Kobayashi, *ibid.* **73**, 132503 (2006); T. Yanagida, Y. Saitoh, Y. Takeda, A. Fujimori, H. Tanaka, and T. Kawai, *ibid.* **79**, 132405 (2009); K. Nagashima, T. Yanagida, H. Tanaka, and T. Kawai, *ibid.* **74**, 172106 (2006); J. Appl. Phys. **100**, 063714 (2006); **101**, 026103 (2007); K. Nagashima, T. Yanagida, K. Oka, and T. Kawai, Appl. Phys. Lett. **94**, 242902 (2009).
[6]Q. Wan, E. N. Dattoli, and W. Lu, Appl. Phys. Lett. **90**, 222107 (2007) ; Q. Wan, J. Huang, Z. Xie, T. Wang, E. N. Dattoli, and W. Lu, *ibid.* **92**, 102101 (2008); E. N. Dattoli, Q. Wan, W. Guo, Y. Chen, X. Pan, and W. Lu, Nano Lett. **7**, 2463 (2007); Q. Wan, E. N. Dattoli, and W. Lu, Small **4**, 451 (2008).
[7]K. Nagashima, T. Yanagida, H. Tanaka, and T. Kawai, Appl. Phys. Lett. **90**, 233103 (2007); J. Appl. Phys. **101**, 124304 (2007); A. Marcu, T. Yanagida, K. Nagashima, H. Tanaka, and T. Kawai, *ibid.* **102**, 016102 (2007); T. Yanagida, K. Nagashima, H. Tanaka, and T. Kawai, Appl. Phys. Lett. **91**, 061502 (2007); J. Appl. Phys. **104**, 016101 (2008); K. Nagashima, T. Yanagida, K. Oka, H. Tanaka, and T. Kawai, Appl. Phys. Lett. **93**, 153103 (2008); K. Nagashima, T. Yanagida, H. Tanaka, S. Seki, A. Saeki, S. Tagawa, and T. Kawai, J. Am. Chem. Soc. **130**, 5378 (2008); A. Marcu, T. Yanagida, K. Nagashima, K. Oka, H. Tanaka, and T. Kawai, Appl. Phys. Lett. **92**, 173119 (2008); T. Yanagida, A. Marcu, H. Matsui, K. Nagashima, K. Oka, K. Yokota, M. Taniguchi, and T. Kawai, J. Phys. Chem. C **112**, 18923 (2008); K. Oka, T. Yanagida, K. Nagashima, H. Tanaka, and T. Kawai, J. Am. Chem. Soc. **131**, 3434 (2009).
[8]F. C. Grozema, L. D. A. Siebbeles, J. M. Warman, S. Seki, S. Tagawa, and U. Scherf, Adv. Mater. **14**, 228 (2002); A. Acharya, S. Seki, Y. Koizumi, A. Saeki, and S. Tagawa, J. Phys. Chem. B **109**, 20174 (2005).
[9]H. Toyosaki, M. Kawasaki, and Y. Tokura, Appl. Phys. Lett. **93**, 132109 (2008).

Downloaded 07 Aug 2009 to 133.1.58.105. Redistribution subject to AIP license or copyright; see http://apl.aip.org/apl/copyright.jsp